Journal of Magnetism and Magnetic Materials 513 (2020) 167250

Contents lists available at ScienceDirect

Journal of Magnetism and Magnetic Materials

journal homepage: www.elsevier.com/locate/jmmm

Research articles

Influence of grain boundaries, interface roughness and non-collinear magnetic configurations in the AF layer on the exchange bias properties of F/AF nanodots: A numerical investigation

Haydar Kanso*, Renaud Patte, Helena Zapolsky, Denis Ledue*

Normandie Université, UNIROUEN, INSA Rouen, CNRS, GPM, F-76800 Saint Étienne du Rouvray, France

ARTICLE INFO

Keywords:
Exchange bias
Roughness
Grain boundaries
Non collinearity
Magnetic domains
Atomic approach

ABSTRACT

Motivated by the insufficient understanding of the drastic effects of the disordered interfacial phases at the interface in F/AF bilayers on the exchange bias properties, we consider a realistic model for F/AF nanodots which accounts for roughness at the interface, grain boundaries (GB) and magnetic frustration in the AF layer. Then, we investigate the effect of the magnetic disorder at the F/AF interface on the exchange field by means of Monte Carlo simulations. First, using a simplified model based on a perfect crystal structure (without GB) and with an ideal interface, our results indicate that non-collinear ordered magnetic configuration at the F/AF interface (due to frustration) causes a small decrease of the exchange field (about few dozen percent). Including GB in the model, we show that this kind of structural disorder produces disordered magnetic configurations with domains at the F/AF interface. This magnetic disorder does not lead to a decrease of the exchange field compared to the perfect crystal but makes the AF layer more stable. Our study also reveals that adding roughness in the form of a percentage of mixed F and AF moments in the interfacial layer results in a more significant decrease of the exchange field (two orders of magnitude) leading to values which are comparable to experimental values.

1. Introduction

The exchange coupling at the interface between ferromagnetic (F) and antiferromagnetic (AF) materials results in a shift of the hysteresis loop along the magnetic field. This phenomenon is known as exchange bias (EB) [1-3] and the shift of the loop is called exchange field (H_E). From a technological point of view, F/AF exchange biased bilayers are used in spintronics devices [4,5], such as magnetic tunnel junction sensors [6] in magnetic random-access memories (MRAM) [7-10] and spin valves [11,12] in read heads [13]. Although EB in F/AF bilayers have been widely investigated in the last decades, from both experimental and theoretical points of view, a full understanding of this phenomenon is still missing. In particular, EB strongly depends on the properties of the F/AF interface where “disordered interfacial phases” or “spin glass like region” have been reported in many experimental works [14-20]. These latter, which can significantly affect the EB properties [16,18,19], are attributed to the combination of structural defects and magnetic frustration at the interface. Similarly, it has been shown that the exchange field decreases as the roughness increases [21,22]. Unfortunately, the magnetic phases at the F/AF interface are hardly accessible by usual experimental techniques and very few models address this point because of its complexity. So, the characterization of the magnetic configuration at the F/AF interface is a puzzling topic and a big challenge, in our days.

Among the numerical studies, a granular approach has been used to model these phases and investigate their effects [23-26]. However, this approach is based on the macrospin approximation and is not able to account for the details at the atomic scale such as structural defects and non-collinearity of the atomic moments. Concerning the atomic approach, some models consider a perfect crystal structure for each layer with an ideal interface [27,28]. In Ref [28] they found that the rotation of the F magnetization applies a torque to the AF moments at the interface which winds up partial domain walls in the antiferromagnet. On the other hand, other models consider structural defects such as non-magnetic impurities or rough interface [29-34]. Among the latter, let us mention the domain state model [29,30] that accounts for non-magnetic impurities in the volume of the AF layer part away from the interface. This model reveals that diluting the AF layer leads to the formation of domains in it which cause and control EB. It should be noted that, in these studies, the Ising model is assumed for the AF material. Within the framework of the domain state model, the influence of an imperfect interface on EB properties has also been investigated [31]. It

* Corresponding author.
E-mail addresses: kansohay@gmail.com (H. Kanso), denis.ledue@univ-rouen.fr (D. Ledue).

https://doi.org/10.1016/j.jmmm.2020.167250
Received 16 April 2020; Received in revised form 12 June 2020; Accepted 17 July 2020
Available online 25 July 2020
0304-8853/ © 2020 Elsevier B.V. All rights reserved.

has been found that H_E (and H_C) strongly depends on the details of the interface and that the AF thickness dependence of rough-interface systems differs significantly from that of ideal-interface systems. More recently, some works have studied the effect of roughness at the F/AF interface on the EB properties by different approaches [22,32-34]. In Refs [22,32,33], it is shown that interfacial roughness reduces the exchange field. In Ref [34], the model is based on the concept of random exchange anisotropy field which acts on the interface AF spins. Then, it has been found that for a single gaussian distribution of the exchange anisotropy field, the exchange field exhibits a maximum around a critical value of the distribution width. Moreover, the exchange field is reduced when the distribution evolves from single gaussian to double gaussian. Also, numerical simulations have shown that interface roughness combined with a small anisotropy in NiO can explain the in-plane perpendicular coupling between NiFe and Co in NiFe/NiO/Co trilayers [35]. Finally, let us mention the Malozemoff's random field model [36-38] which has demonstrated that the presence of random interface roughness gives rise to AF domain walls perpendicular to the interface and an exchange anisotropy below a critical AF thickness $t_c^{(1)}$. More precisely, between $t_c^{(1)}$ and a second critical AF thickness $t_c^{(2)}$ ($t_c^{(2)} < t_c^{(1)}$), the exchange field is constant while it is proportional to $1/t_{AF}$ below $t_c^{(2)}$.

To our knowledge, only one study has considered a F layer coupled to a spin glass [39] (modeled by the Ising model) and its influence on the hysteresis loop. Then, it was observed that EB results from a frozen spin-glass state and the exchange field decreases with increasing strength of the cooling field in qualitative agreement with experimental results. We would like to emphasize that there are no studies dealing with the effect of grain boundaries (GB) on the EB properties.

In this work, our goal is to model magnetic disorder (with canted moments) at the F/AF interface using a realistic model for F/AF nanodots which accounts for GB, roughness at the interface and magnetic frustration in the AF layer. Then, we investigate its effects on the EB properties. To that purpose, our strategy is to improve our model step by step. (i) First, we consider a perfect crystal structure (without GB) for each layer with an ideal interface in a preliminary study. (ii) Then, in order to study only the effect of GB in presence of magnetic frustration in the AF layer, we consider a bilayer with GB and an ideal interface. (iii) Finally, we consider a more realistic bilayer with a rough interface in addition to the presence of GB. In each case, we quantify the influence of the canting of the magnetic moments at the interface on the exchange field in terms of an effective interlayer coupling and on the stability of the AF layer, *i.e.* if it reverses with the F layer. To that purpose, we use an atomic approach and Monte Carlo simulations [40]. The interest of the Monte Carlo method is to account for the thermal fluctuations of the magnetic moments. The atomistic modelling of GB structure is performed using the quasiparticle approach [41] which is based on the atomic function density (ADF) theory [42]. In the past, this method has been used successfully to study the GB structure and the segregation phenomena at GB 1 [43-45].

The remainder of the paper is organized as follows. The model and simulation details are described in Sec. II. Numerical results and discussion are presented in Sec. III. Finally, the conclusion is given in Sec. IV.

2. Model and simulation

Our model for a F/AF nanodot consists of two layers with body-centered cubic structure (BCC). The F layer contains two atomic planes and the AF layer contains four atomic planes. In order to study the effect of GB on the EB properties, we have generated two kinds of BCC structures: a perfect BCC structure and a BCC structure with GB. Moreover, we have considered two types of interface: an ideal interface without mixing and a rough interface with one atomic plane containing F and AF atoms.

The atomic structure of the symmetric tilt GB Σ5(031) [001] θ = 36.87°, frequently observed in BCC metals, was simulated using the quasiparticle approach [41]. In this method, we assume that the distance between the atoms is larger than the computation grid. Then each atom is associated to a sphere comprised of some number of simulation grids which are atomic fragments. These fragments are treated as pseudo-particles and are named "fratons". In this description, the dynamics of the system is described by a creation or annihilation of a "fratons": a creation of a "fraton" at a point, r, indicates that atomic movements resulted in a situation wherein the point r, which was previously outside of any atomic spheres, turned out inside of one of them; annihilation of a "fraton" describes an opposite process wherein the point, r, which initially is within of an atomic sphere, becomes outside of it. Unlike the conventional approach describing the configuration of a multi-atomic system by coordinates of atomic centres, the quasi-particle approach describes atomic configurations by occupation numbers of "fratons". The proper choice of a model Hamiltonian describing the interaction of "fratons" should result in both creation of atomic spheres and the movement of the spheres into the desirable equilibrium atomic configuration driven by the spontaneous minimization of the free energy. The variable, that determines the atomic configurations, is the occupation probability function $\rho_\alpha(\boldsymbol{r},t)$ which is the probability, that point $\boldsymbol{r}$, is inside the atomic sphere of any atom of the kind α at the time t. A temporal and spatial dependence of $\rho_\alpha(\boldsymbol{r},t)$, describes the evolution of the atomic configurations:

$$\frac{d\rho_\alpha(\boldsymbol{r},t)}{dt} = \sum_{\boldsymbol{r}'} \sum_{\beta=1}^{\beta=m} \frac{L_{\alpha\beta}(\boldsymbol{r}-\boldsymbol{r}')}{k_B T} \frac{\delta G}{\delta \rho_\beta(\boldsymbol{r}',t)} \tag{1}$$

where $L_{\alpha\beta}(r)$ is the matrix of kinetic coefficients, the summation is carried out over all grid sites, k_B is the Boltzmann constant, T is temperature, and G is the non-equilibrium Gibbs free energy functional. The Gibbs free energy was interpolated by the equation for the mean field free energy:

$$G = \frac{1}{2}\sum_{r,r'}\sum_{\alpha=1}^{\alpha=m}\sum_{\beta=1}^{\beta=m} W_{\alpha\beta}(r-r')\rho_\alpha(r)\rho_\beta(r') + k_B T \sum_r \left[\sum_{\alpha=1}^{\alpha=m}\rho_\alpha(r) ln\rho_\alpha(r) + \left(1-\sum_{\alpha=1}^{\alpha=m}\rho_\alpha(r)\right) ln\left(1-\sum_{\alpha=1}^{\alpha=m}\rho_\alpha(r)\right)\right] \tag{2}$$

where $W_{\alpha\beta}(\boldsymbol{r}-\boldsymbol{r}')$ is the model potential of interaction of the pair of "fratons" of the components α and β , respectively, where $\boldsymbol{r}$ and $\boldsymbol{r}'$ are positions of the grid sites occupied by the "fratons" of this pair. Summation over $\boldsymbol{r}$ and r' in Eqs. (1) and (2) is carried out over the N sites of the computational grid lattice. The simulation was performed with the mean density of "fraton" $\bar{\rho} = 0.104$ in the 3D simulation box with 600 × 600 × 64 unit cells. The lattice parameter of the BCC crystal used in the simulations has been adjusted to model a typical BCC structure. Eq. (1) was solved in 3D using semi-implicit Fourier-spectral method. The details of this resolution are given in Ref[41].

The obtained atomic configuration of the symmetric tilt GB Σ5(031) [001] is shown in Fig. 1. This GB structure can be described by the structural units B [45] characterized by low energy. This why this GB are frequently observed in different BCC crystals.

In order to investigate the effect of magnetic disorder with canted moments at the F/AF interface, we have considered the Heisenberg model where the spins $\boldsymbol{S}_i$ can take any orientation in the space. Our magnetic Hamiltonian contains three terms: the exchange energy, the anisotropy energy and the Zeeman energy. The exchange energy can be written as:

$$E_{ech} = -J_F \sum_{<i,j>\in F} \boldsymbol{S}_i.\boldsymbol{S}_j - J_1^{AF} \sum_{<i,j>\in AF} \boldsymbol{S}_i.\boldsymbol{S}_j - J_2^{AF} \sum_{<i,j>\in AF} \boldsymbol{S}_i.\boldsymbol{S}_j - J_{int} \sum_{i\in F, j\in AF} \boldsymbol{S}_i.\boldsymbol{S}_j$$

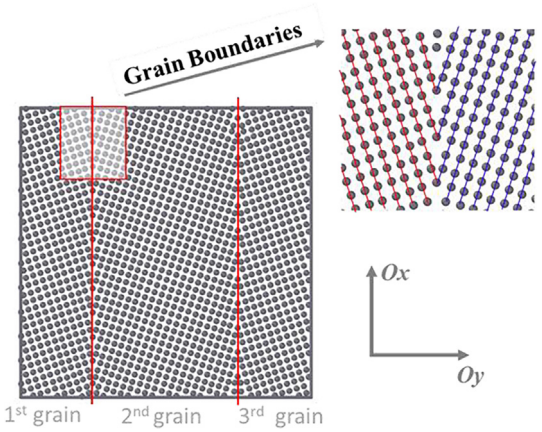


Fig. 1. Structure of the Σ5(031) [001] tilt GB in the BCC Fe obtained using the quasiparticle approach. The structure is viewed along the [100] tilt axis. The magnified view of GB region shows the structural units B (black and gray denote atoms on different {100} planes).

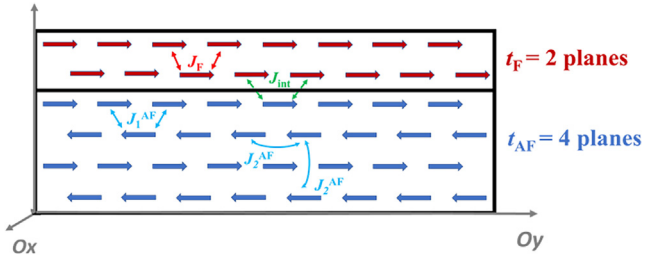


Fig. 2. Sketch of the model with an ideal interface and without grain boundaries showing the exchange interactions. The F layer contains two planes and the AF layer contains four planes. Note that the directions of the magnetic moments correspond to the ground state if $J_2^{AF} = 0$ (no frustration).

Table 1
Constant parameters in our simulations.

S_F = 0,85	D_F = 1 K	J_F = 910 K	T_C = 1360 K
S_{AF} = 1	D_{AF} = 10 K	J_1^{AF} = − 335 K	T_N = 690 K

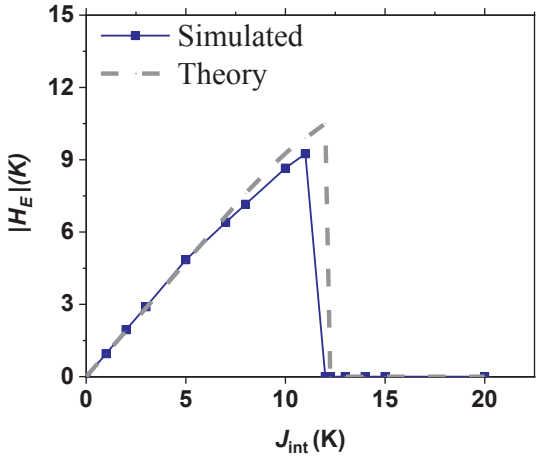


Fig. 3. Variation of H_E simulated at $T = 0.1$ K versus J_{int} in comparison with the theoretical values given by Eq. (4) ($J_2^{AF} = 0$ K).

where $J_F > 0$ is the nearest-neighbor (NN) interaction between two F atoms, $J_{int} > 0$ is the NN interaction between a F and an AF atom and, J_1^{AF} and J_2^{AF} are the NN and NNN (next nearest-neighbor) interactions

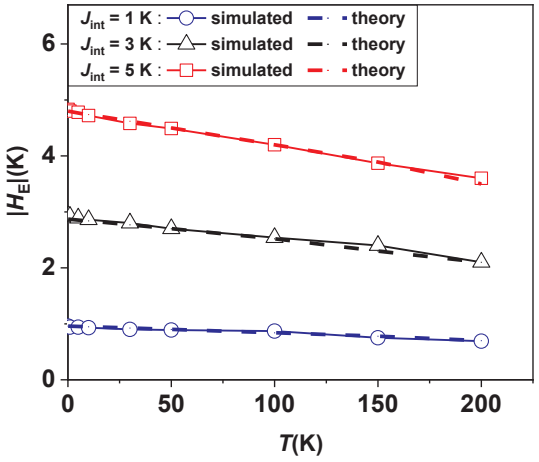


Fig. 4. Temperature dependence of H_E for different values of J_{int} in comparison with the generalized expression of H_E (Eq. (6)) ($J_2^{AF} = 0$ K).

between two AF atoms (Fig. 2). J_1^{AF} is assumed to be negative to model the AF material. Then, if $J_2^{AF} = 0$, the AF moments of an atomic plane are parallel and the magnetizations of two adjacent planes are antiparallel (Fig. 2). Likewise, J_2^{AF} is negative in order to generate magnetic frustration which is necessary to obtain non-collinear magnetic configurations. Assuming an uniaxial anisotropy along a common easy axis (Oy) in the plane of the layer, the anisotropy energy is:

$$E_a = -D_F \sum_{i\in F} (S_i^y)^2 - D_{AF} \sum_{i\in AF} (S_i^y)^2$$

where $D_F > 0$ and $D_{AF} > 0$ are respectively the anisotropy constant per atom for the F and AF atoms. Let us mention that such a magnetic texture can be obtained by applying an external field along the y-axis during the fabrication of the samples.

he Zeeman energy is given by:

$$E_Z = \mu_0 \mu_B \boldsymbol{H}. \sum_i g_i \boldsymbol{S}_i$$

Most parameters of our model can be estimated from the literature. The exchange interaction J_F is chosen in such a way that the Curie temperature of the F material is that of cobalt, *i.e.* $T_C = 1360$ K [46]. Since for the Heisenberg model on the (infinite) BCC lattice [47], one has:

$$\frac{k_B T_C}{J_F S_F^2} \approx 2.054 \qquad (3)$$

we find $J_F = 1.256 \times 10^{-20}$ J for $S_F = 0.85$. The value of the anisotropy constant per atom is $D_F = 1.1 \times 10^{-23}$J [48]. Concerning the AF material, we assume that its Néel temperature is that of $IrMn_3$, *i.e.* $T_N = 690$ K [46]. So, using Eq.(3) again with $S_{AF} = 1$, we find $J_1^{AF} = -4.63 \times 10^{-21}$J. In this work, the coupling $J_2^{AF} < 0$ is variable and we consider $|J_2^{AF}| \leq 0.6\,|J_1^{AF}|$. The value of the anisotropy constant per atom is taken to be $D_{AF} = 10\,D_F$. For practical reasons, the magnetic parameters are divided by k_B (J_{ij}/k_B et D/k_B) and are thus given in Kelvin (K). Also, in the following results, the exchange field H_E is expressed in Kelvin (which corresponds to $\frac{\mu_0 \mu_B H_E}{k_B}$). The parameters which are constants in all our simulations are summarized in Table 1.

The stable magnetic configurations of the nanodots at low temperature have been obtained by a simulated annealing based on the standard Metropolis algorithm [49]. For that, the simulation starts at high enough temperature T_1 (*i.e.* above the transition temperature of the finite F layer), here $T_1 = 800$ K, and decreases according to the law $T_{n+1} = T_n - \Delta T$ with $\Delta T = 5$ K with a final temperature equal to 0.1 K. The hysteresis loops were simulated using the same algorithm combined with the time step quantified MC method [50,51]. Simulations were performed with 1600 atoms per plane for the perfect BCC

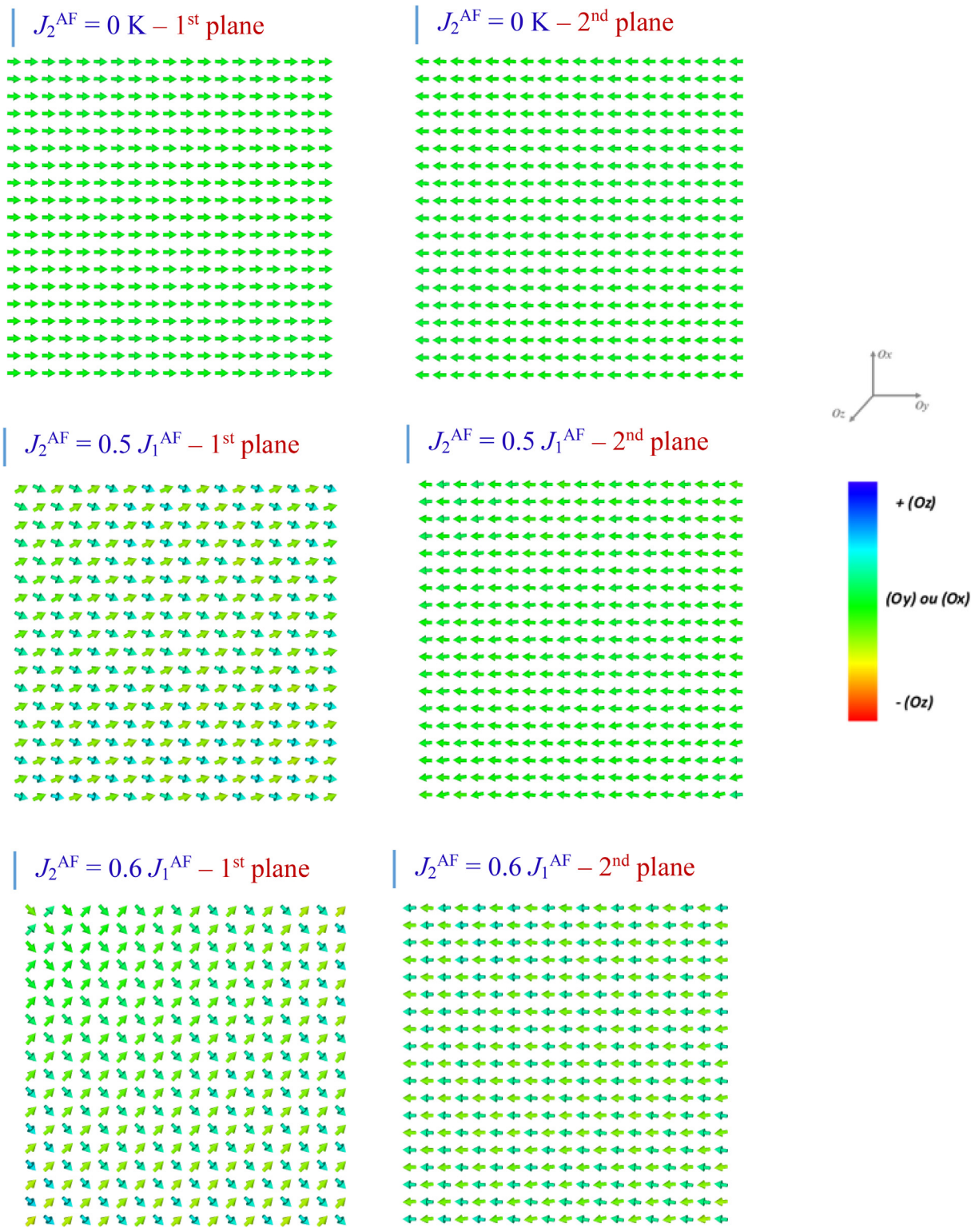


Fig. 5. Central part (19 × 19 atoms) of the magnetic configurations at $T = 0.1$ K of the first and second planes of the perfect BCC AF layer for different values of J_2^{AF}. The color code represents the component of the magnetic moments along the axis perpendicular to the plane (z-axis). A moment that is in the plane is green with a maximal length. (For interpretation of the references to color in this figure legend, the reader is referred to the web version of this article.)

structure and with 1461 for the BCC structure with GB.

3. Results and discussions

3.1. Perfect BCC structure with an ideal interface

3.1.1. Bilayer without magnetic frustration ($J_2^{AF} = 0$)

In order to check the reliability of our simulations, we consider a

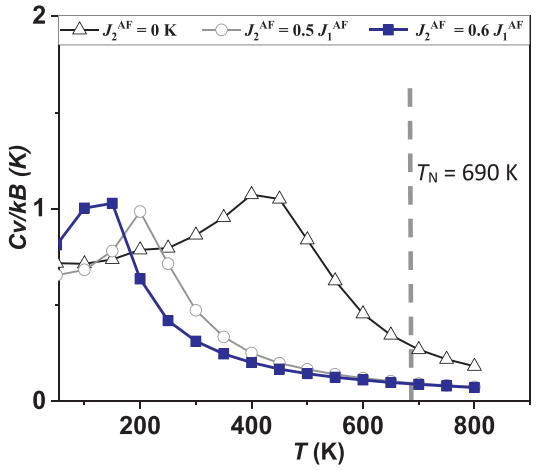


Fig. 6. Temperature dependence of the specific heat of the AF layer for different values of J_2^{AF}.

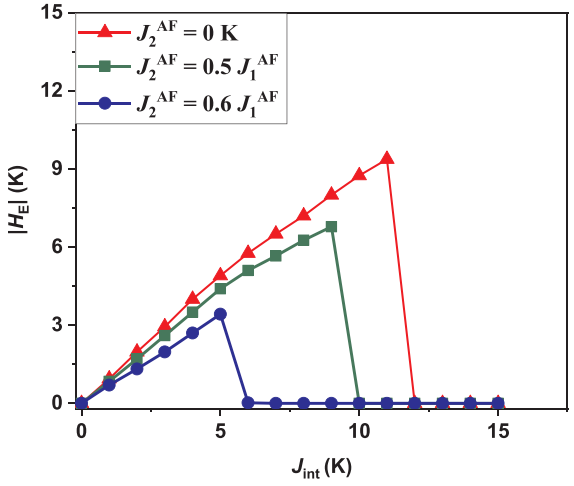


Fig. 7. Variation of H_E simulated at $T = 0.1$ K versus J_{int} for different values of J_2^{AF}.

perfect BCC crystal (without GB) with an ideal interface and without frustration ($J_2^{AF} = 0$). Since in that case the F layer with $t_F = 2$ planes should reverse at 0 K by uniform rotation, we can compare our results with those of the Meiklejohn and Bean model [1]. In this model the

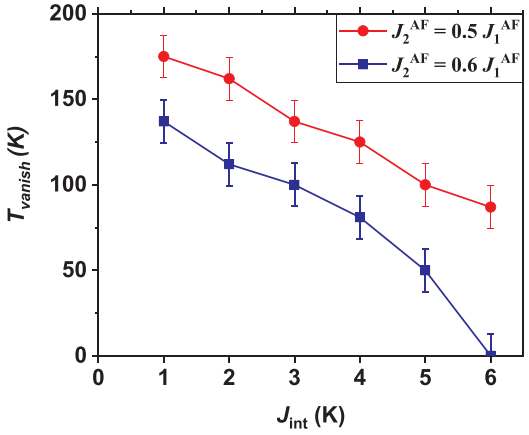


Fig. 9. Variation of T_{vanish} versus J_{int} for $J_2^{AF} = 0.5\ J_1^{AF}$ and $J_2^{AF} = 0.6\ J_1^{AF}$.

exchange field at 0 K is given by :

$$\mu_0 \mu_B H_E = -\frac{Z_{F-AF} S_{AF} J_{int}}{N_F g_F} \quad (4)$$

where $Z_{F\text{-}AF}$ is the number of F-AF bonds at the interface and N_F the number of atoms in the F layer, and the non-reversal criterion for the AF layer is :

$$N_{AF}\ D_{AF}\ S_{AF} > Z_{F\text{-}AF}\ J_{int}\ S_F \quad (5)$$

where N_{AF} is the number of atoms in the AF layer. In our simulations, the F layer reverses by uniform rotation for all values of J_{int}. Also, we have observed that the AF and F moments rotate together for $J_{int} \geq 12$ K. The comparison between the simulated values of H_E (at $T = 0.1$ K) versus J_{int} and the theoretical values given by Eq. (4) is shown in Fig. 3.

For $J_{int} \leq 5$ K the exchange field increases linearly with J_{int} and there is an excellent agreement with Eq. (4) which indicates that our results are reliable. For 5 K $< J_{int} <$ 12 K, there is a small shift from Eq. (4) because of AF moment rearrangements at the interface when the F layer reverses which are not taken into account in Eq. (4). For $J_{int} \geq 12$ K, H_E vanishes since the AF layer reverses with the F layer. Again, we found a good agreement with the non-reversal condition of the AF layer (Eq. (5)) which predicts that the AF layer should reverse with the F one if $J_{int} \geq 12.25$ K.

Subsequently, we simulated the temperature dependence of the exchange field to see if Eq. (4) (which is valid only at 0 K) can be generalized at $T \neq 0$ K by replacing S_{AF} with the thermal average of the

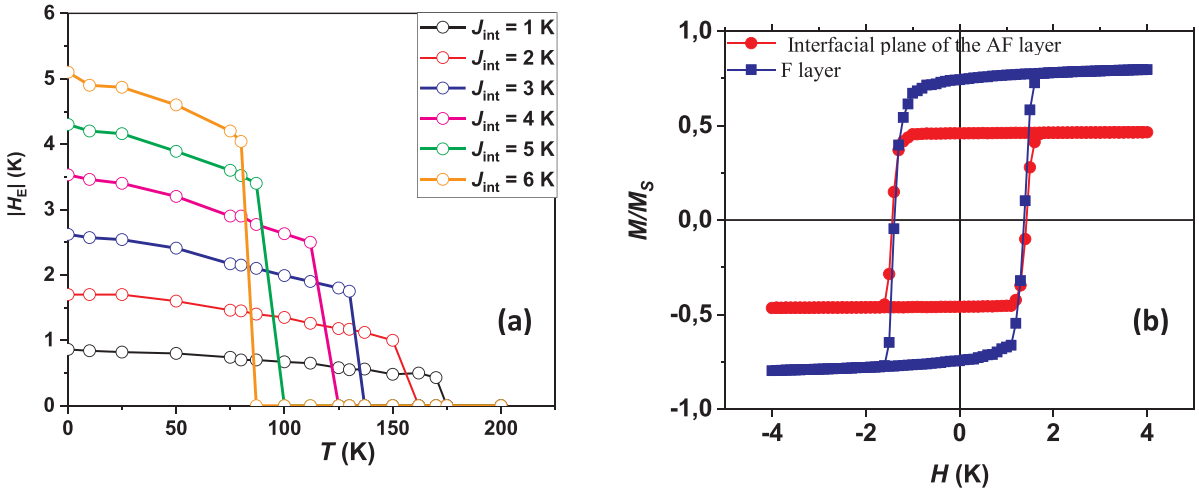


Fig. 8. (a) Temperature dependence of H_E for $J_2^{AF} = 0.5\ J_1^{AF}$ and various values of J_{int}, (b) hysteresis loops at $T = 175$ K for $J_{int} = 3$ K.

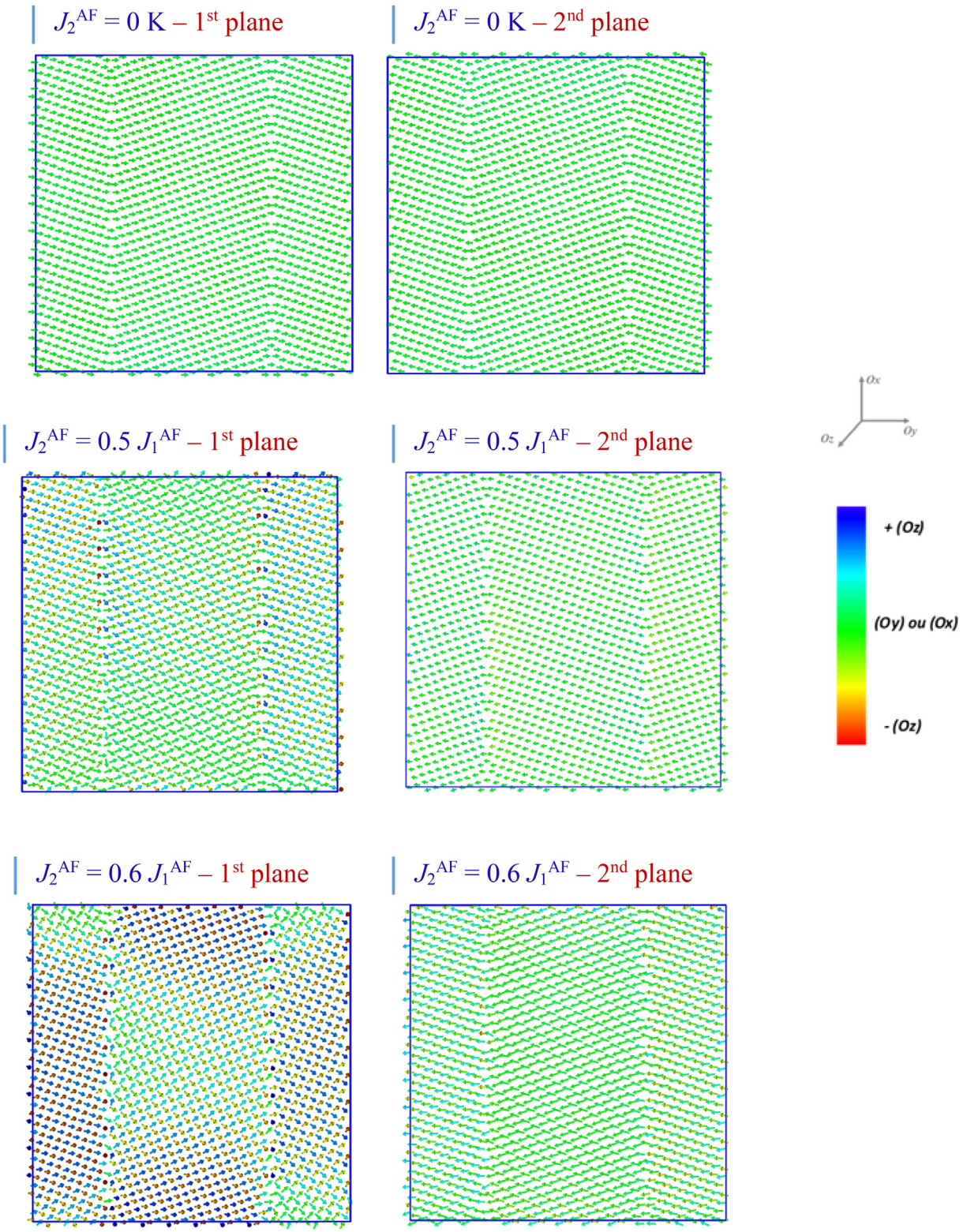


Fig. 10. Magnetic configurations at 0.1 K of the first and second planes of the BCC AF layer with GB for different values of J_2^{AF}. The color code represents the component of the magnetic moments along the axis perpendicular to the plane (*z*-axis).

component of the AF spin at the interface along the direction of the applied field (here the *y* axis), $<S_{AF}^{y}>_T$:

$$\mu_B \mu_0 H_E(T) = -\frac{Z_{F-AF}}{N_F g_F} J_{int} < S_{AF}^{y} > T \quad (6)$$

It is important to note that $<S_{AF}^{y}>_T$ decreases as T increases due to thermal fluctuations. In Fig. 4, we plot the temperature dependence of H_E for J_{int} = 1, 4 and 5 K in comparison with Eq. (6) in which $<S_{AF}^{y}>_T$ has been calculated by numerical simulations. It can be seen that H_E decreases as T increases with a very good agreement with Eq. (6). So, the Meiklejohn and Bean formula can be generalized at non-zero temperature by Eq. (6) which clearly links the decrease of H_E to the thermal

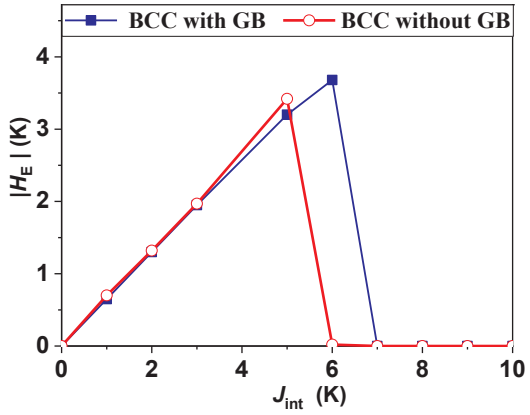


Fig. 11. Variation of H_E simulated at 0.1 K versus J_{int} for a BCC nanodot with GB in comparison with a perfect BCC nanodot ($J_2^{AF} = 0.6\ J_1$).

fluctuations of the AF moments at the interface.

3.1.2. Bilayer with magnetic frustration ($J_2^{AF} \neq 0$)

With the goal of generating non-collinear magnetic configurations in the AF layer which requires magnetic frustration, we account for a negative second neighbors ($J_2^{AF} < 0$) in addition to J_1^{AF}. First, we present the effect of J_2^{AF} on the magnetic configurations of the AF layer at 0.1 K and on the transition temperature of the AF layer, then we study the effect of J_2^{AF} on the J_{int}- and temperature dependencies of the exchange field.

3.2. Effect of J_2^{AF} on the magnetic configurations at 0.1 K and on the transition temperature of the AF layer

The magnetic configurations of the first plane (interfacial plane) and the second one of the AF layer obtained after cooling ($T_f = 0.1$ K) are presented in Fig. 5 for different values of J_2^{AF}. As expected, for $J_2^{AF} = 0$ K, the two planes are F (with opposite magnetizations) since there is no frustration. For $J_2^{AF} = 0.5\ J_1^{AF}$ and $0.6\ J_1^{AF}$, the magnetic moments of the interfacial plane are non-collinear but they are still forming a single domain. However, the second plane is F as for the case $J_2^{AF} = 0$ K. Since the stable configurations in the infinite BCC crystal with interactions up to the second neighbors are always collinear [46], the magnetic configurations observed here in the first plane comes from the combined effect of the frustration and the interface. We also study the effect of J_2^{AF} on the transition temperature (T_N) of the AF layer. In Fig. 6, we plot the temperature dependence of the specific heat, which exhibits a peak at T_N, for different values of J_2^{AF}. For $J_2^{AF} = 0$ K, the peak is located at $\approx$ 400 K, well below 690 K because of finite-size effects. As $|J_2^{AF}|$ increases, the peak shifts towards lower temperature due to the increase of magnetic frustration. For $|J_2^{AF}| = 0.6\ |J_1^{AF}|$, the peak is located at $\approx$ 150 K.

3.3. Effect of J_2^{AF} on the exchange field at 0.1 K

In Fig. 7, we present the variation of H_E simulated at $T = 0.1$ K versus J_{int} for different values of J_2^{AF}, *i.e.* for various magnetic configurations of the first plane of the AF layer.

Qualitatively, the same behavior of H_E is observed for all values of J_2^{AF}: H_E increases (almost linearly) if J_{int} is small and vanishes at a critical value of J_{int} because the AF moments follow the motion of the F layer. However, there are two effects due to the increase of J_2^{AF}. (i) For small values of J_{int}, H_E decreases as $|J_2^{AF}|$ increases due to the non-collinearity of the AF moments at the interface. So, the non-collinearity of the AF moments at the interface results in a decrease of the effective F/AF coupling at the interface. (ii) The critical value of J_{int} above which the AF layer reverses with the F layer decreases as $|J_2^{AF}|$ increases ($J_{int} = 12$ K for $J_2^{AF} = 0$ K and $J_{int} = 6$ K for $J_2^{AF} = 0.6\ J_1$). According to Eq. (5), it means that either the effective F/AF coupling increases or the effective AF anisotropy constant (*i.e.* the energy barrier to overcome by the AF layer when it reverses) decreases. From (i), only the decrease of the effective AF anisotropy constant is possible. To summarize, the non-collinearity of the AF moments at the interface decreases the effective F/AF coupling and the effective AF anisotropy constant.

3.4. Effect of J_2^{AF} on the temperature dependence of the exchange field

In this part, we study the temperature dependence of the exchange field for different values of J_{int} when $J_2^{AF} = 0.5\ J_1^{AF}$ and $J_2^{AF} = 0.6\ J_1^{AF}$. The variation of H_E for $J_2^{AF} = 0.5\ J_1^{AF}$ is plotted in Fig. 8.a. Unlike the case $J_2^{AF} = 0$ K (Fig. 4), H_E vanishes at a temperature T_{vanish} which varies from 175 K to 85 K as J_{int} decreases. It is important to note that for all values of J_{int}, T_{vanish} is smaller than T_N ($\approx$ 200 K for $J_2^{AF} = 0.5\ J_1$). For $T < T_{vanish}$, the values of H_E are slightly smaller than those of $J_2 = 0$ K (see Fig. 4), due to the non-collinearity of the AF magnetic moments at the interface. As shown in Fig. 8.b, for $T_N > T \geq T_{vanish}$, the AF layer reverses with the F layer thus H_E is equal to zero. If we assume that T_{vanish} is a blocking temperature, the decrease of T_{vanish} as J_{int} increases can be explained by a lowering of the barrier to overcome by the AF layer during its reversal.

The variation of T_{vanish} versus J_{int} for $J_2 = 0.6\ J_1$ and $J_2 = 0.5\ J_1$ is plotted in Fig. 9. We find that $T_{vanish}(J_2^{AF} = 0.6\ J_1^{AF}) < T_{vanish}(J_2^{AF} = 0.5\ J_1^{AF})$ which indicates that the energy barrier to overcome by the AF layer is smaller for $J_2^{AF} = 0.6\ J_1^{AF}$.

3.5. BCC nanodot with grain boundaries, ideal interface and $J_2^{AF} \neq 0$

Our goal is to understand the effect of GB on the magnetic configurations in the AF layer at 0.1 K and on the exchange field by comparing these results with those obtained in Sec.A.2 without GB.

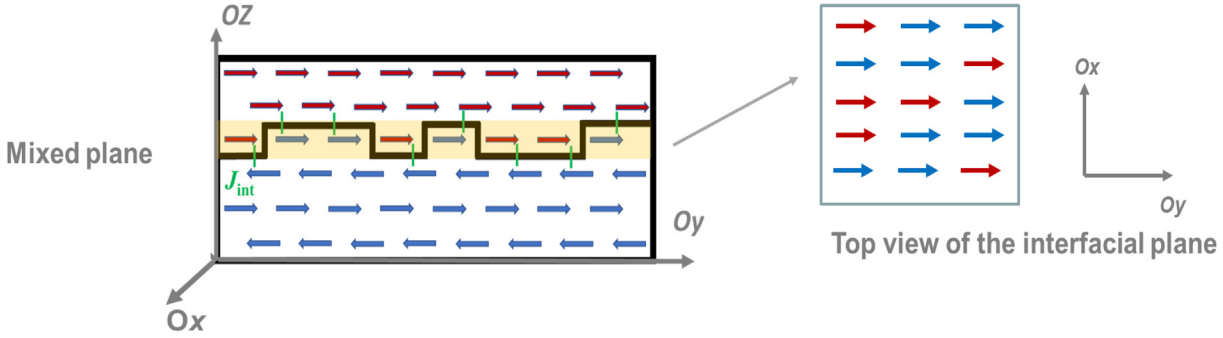


Fig. 12. F/AF nanodot with roughness at the interface. Red arrows represent the F moments and the blue arrows represent the AF moments. Note that the direction of the magnetic moments in the mixed plane and in the AF layer depends on the percentage of F moments in this plane. (For interpretation of the references to color in this figure legend, the reader is referred to the web version of this article.)

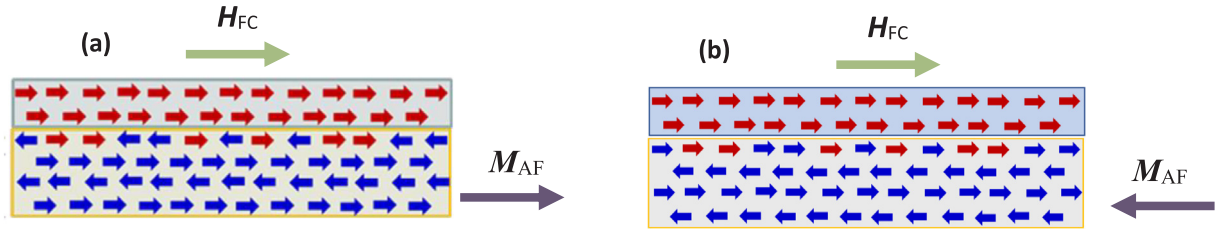


Fig. 13. F/AF nanodot with roughness at the interface. Red arrows represent the F moments and blue arrows represent the AF moments. (a) The AF moments of the mixed plane point toward the left and the net magnetization of the AF layer points toward the right and (b) the AF moments of the mixed plane point toward the right and the net magnetization of the AF layer points toward the left. (For interpretation of the references to color in this figure legend, the reader is referred to the web version of this article.)

3.6. Effect of the grain boundaries on the magnetic configurations of the AF layer at 0.1 K

The magnetic configurations of the first plane (interfacial plane) and the second one of the AF layer with GB obtained after cooling down to $T_f = 0.1$ K are shown in Fig. 10 for different values of J_2^{AF}. As expected, for $J_2^{AF} = 0$ K, the planes are F with antiparallel magnetizations since there is no frustration. For$J_2^{AF} = 0.5\ J_1$, the magnetic moments of the interfacial plane are non-collinear, in addition to that some moments which are localized at the GB and at the edges are out of the plane (*Oxy*). However, the second plane is still F. For $J_2^{AF} = 0.6\ J_1$, we observe that the fraction of magnetic moments out of plane at the interface increases. Unlike the case of a BCC nanodot without GB, there are several magnetic domains in the interfacial plane and each grain contains several domains. The magnetic moments of the second plane are no more collinear but are still contained in the *xy* plane. So, the combined effect of GB, interface and frustration generate disordered magnetic configurations with domains.

3.7. Effect of the grain boundaries on the exchange field at 0.1 K

In this part, we investigate the effect of GB on the variation of H_E simulated at $T = 0.1$ K versus J_{int} for $J_2^{AF} = 0.6\ J_1^{AF}$ (Fig. 11). It can be seen that the values of H_E of the BCC nanodot with GB are the same as in the case of the perfect BCC nanodot (as long as the AF layer does not reverse). The only difference between the two curves of Fig. 11 is the value of J_{int} for which H_E vanishes which is slightly higher when there are GB in the layers ($J_{int} = 7$ K in case of GB and $J_{int} = 6$ K without GB). So, our simulations show that GB make the AF layer more stable at 0 K, *i.e.* the effective anisotropy constant of the AF layer is increased by the GB.

3.8. BCC nanodot with grain boundaries, a rough interface and $J_2^{AF} = 0$

In this part, we study the effect of roughness at the interface on the magnetic configurations in the AF layer at 0.1 K and on the exchange field. The first plane of the AF layer (interfacial plane) contains F and AF moments which are randomly distributed (Fig. 12). The percentage of the F moments in this plane is x_F. Here, we have considered $J_2^{AF} = 0$ K but we would like to emphasize that due to roughness there is magnetic frustration at the interface.

3.9. Effect of x_F on the magnetic configurations at 0.1 K ($J_2^{AF} = 0$ K)

We remind that for $x_F = 0\%$ and $J_2^{AF} = 0$ K, the AF moments at the interface are in the same direction as the F layer magnetization, that is along $\boldsymbol{H}_{FC}$ (to the right), because of $J_{int} > 0$ (see Fig. 10). The magnetizations of two neighboring planes in the AF layer are anti-parallel and so, the net magnetization of the AF layer $\boldsymbol{M}_{AF}$ is equal to zero. For $x_F \neq 0\%$, $\boldsymbol{M}_{AF}$ is no longer equal to zero and is opposite to the AF moments of the mixed plane (Fig. 13). Since the cooling field $\boldsymbol{H}_{FC}$ favors $\boldsymbol{M}_{AF}$ to the right, *i.e.* the AF moments of the mixed plane to the left (configuration of Fig. 13.a), and J_{int} favors the AF moments of the mixed plane to the right (configuration of Fig. 13.b), there is a competition between J_{int} and $\boldsymbol{H}_{FC}$.

The magnetic configurations of the mixed plane (interfacial plane) obtained after cooling under a positive field H_{FC} down to $T_f = 0.1$ K are shown in Fig. 14 for different values of x_F (20%, 40% and 50%) and $J_{int} = 20$ K. For $20\% \leq x_F \leq 40\%$, the AF moments of the mixed plane are along $\boldsymbol{H}_{FC}$, so $\boldsymbol{M}_{AF}$ is opposite to $\boldsymbol{H}_{FC}$, which means that the effect of J_{int} dominates the effect of $\boldsymbol{H}_{FC}$ (Fig. 14.a & 14.b). We note that for $x_F \geq x_c \approx 50\%$, the AF moments of the mixed plane are in the opposite direction from $\boldsymbol{H}_{FC}$, so $\boldsymbol{M}_{AF}$ is along $\boldsymbol{H}_{FC}$, which means that the effect of $\boldsymbol{H}_{FC}$ dominates (Fig. 14.c). So, we observe a drastic change in the magnetic configuration of the mixed plane from F to almost AF as x_F goes from 20% to 50%. Since the magnetic configuration of the (mixed) interfacial plane has a strong influence on H_E, it is expected that H_E varies strongly with x_F.

3.10. Effect of x_F on the exchange field at 0.1 K ($J_2^{AF} = 0$ K)

Now, we study the effect of x_F on the J_{int} - dependence of H_E at $T = 0.1$ K with$J_2^{AF} = 0$ K. It is important to note that with roughness, there are two opposite contributions to H_E : a contribution due to the AF moments of the mixed plane and another one due to the AF moments of the second plane of the AF layer (just below the mixed plane) which interacts with the F moments of the mixed plane (see Fig. 12). For $x_F < x_c \approx 50\%$, the AF moments of the mixed plane give a negative contribution to H_E whereas the AF moments of the second plane of the AF layer give a positive contribution. It is the contrary for $x_F = 50\%$.

Below x_c, H_E is negative and $|H_E|$ decreases as x_F increases (as long as the AF layer does not reverse) (Fig. 15.a) since the number of F-AF bonds between the interfacial plane of the F layer and the mixed plane (which give a negative contribution to H_E) decreases and the number of the F-AF bonds between the mixed plane and the first pure plane of the AF layer (which give a positive contribution to H_E) increases. So, roughness decreases the effective coupling at the interface. To analyze quantitatively our results, we calculate the theoretical value of the exchange field assuming that the AF moments are pinned and neglecting the lack of bonds at the edges. Then, generalizing Eq. (4), we obtain:

$$\mu_0 \mu_B H_E = -\frac{4(1 - 2x_F) S_{AF} J_{int}}{(2 + x_F) g_F} \tag{7}$$

So, we plot $\mu_0\ \mu_B\ g_F\ |H_E|\ /\ (4\ S_{AF}\ J_{int})$ versus x_F in order to see if all data points are on a single curve of equation $(1–2\ x_F)/(2\ +\ x_F)$. As seen in Fig. 15.b, our results are in reasonable agreement with Eq. (7) which shows that the decrease of $|H_E|$ as x_F increases can be mainly explained by the variation of the number of F-AF bonds at the interface. It should be noted that the data points which slightly deviate from the theoretical curve are those for which they are AF moment rearrangements during the reversal of the F layer (*i.e.* for values of J_{int} just below the critical value for which the AF layer reverses with the F one). For $x_F = 50\% \geq x_c$, H_E becomes positive but is very small in comparison with that

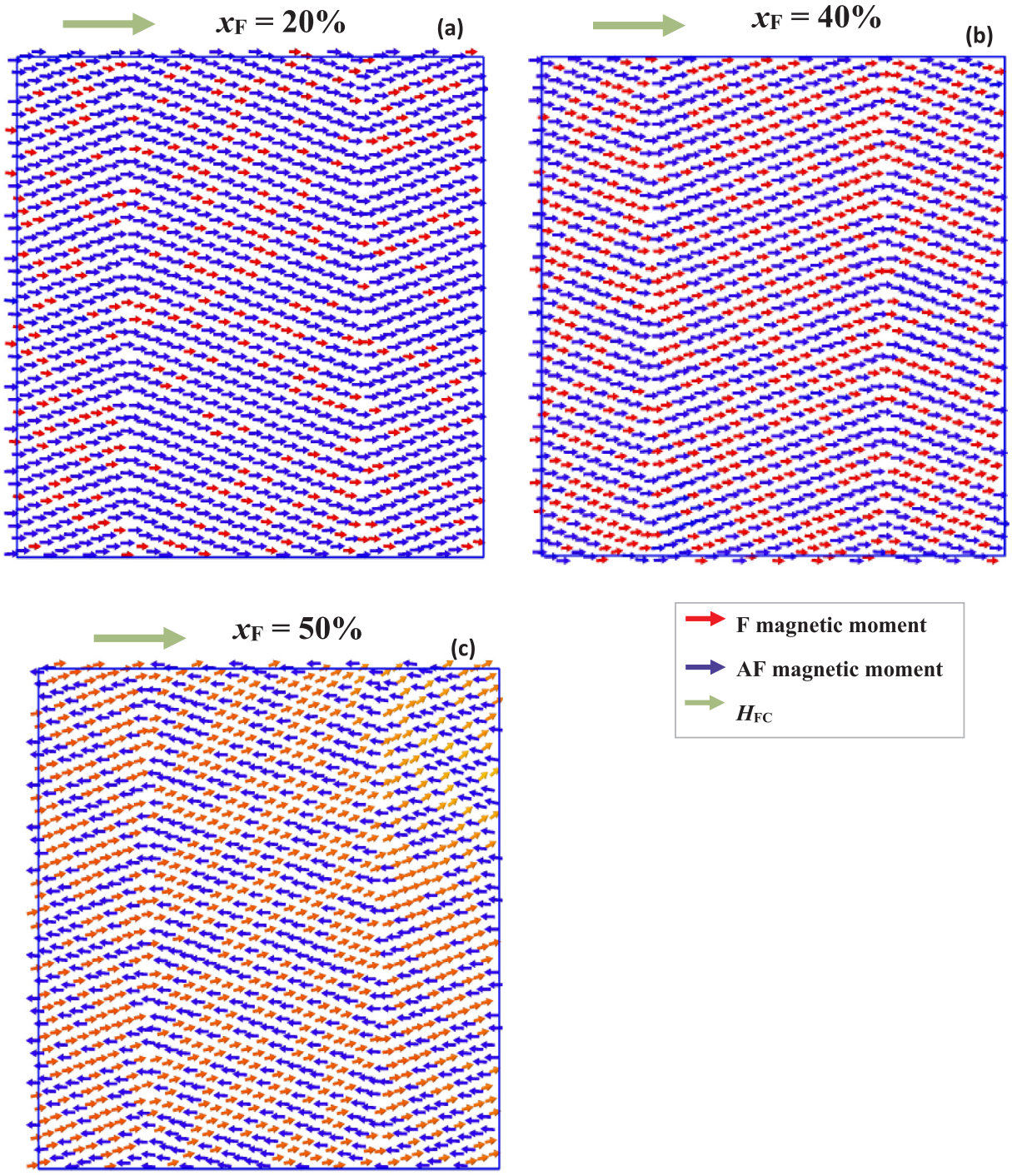


Fig. 14. Magnetic configurations at 0.1 K of the mixed plane with GB for different values of x_F ($J_2^{AF} = 0$ K and $J_{int} = 20$ K). For $x_F = 20$ and 40%, the AF moments of the mixed plane are along $\boldsymbol{H}_{FC}$ whereas for $x_F = 50\%$, the AF moments of the mixed plane are in the opposite direction from $\boldsymbol{H}_{FC}$.

obtained for $x_F \leq 40\%$ (Fig. 16) because the two opposite contributions almost compensate each other. We point out that the simulated values of H_E in this case (50%) are comparable to the experimental values. For example, for $J_{int} = 20$ K, the simulated value is $H_E = 1600$ Oe for two F atomic planes, *i.e.* $t_F \approx 0.5$ nm. Since H_E is proportional to $1/t_F$, H_E will be equal to 160 Oe for a F layer with $t_F = 5$ nm which fits very well with the experimental values. So, our results indicate that it is possible to simulate realistic values of the exchange field using an atomic approach with realistic exchange interactions which accounts for roughness at the interface.

4. Conclusion

In this paper, we modeled non-collinear magnetic configurations at the F/AF interface in the AF layer using either a perfect crystal structure or a crystal structure with GB. Our numerical simulations showed that ordered non-collinear configurations at the F/AF interface observed in the perfect crystal results in a small decrease of the exchange field. When considering GB in the model, the magnetic configurations at the F/AF interface are disordered with domains but do not lead to lower value of the exchange field compared to the perfect crystal. However, the AF layer with GB is more stable than the perfect one. Finally, our

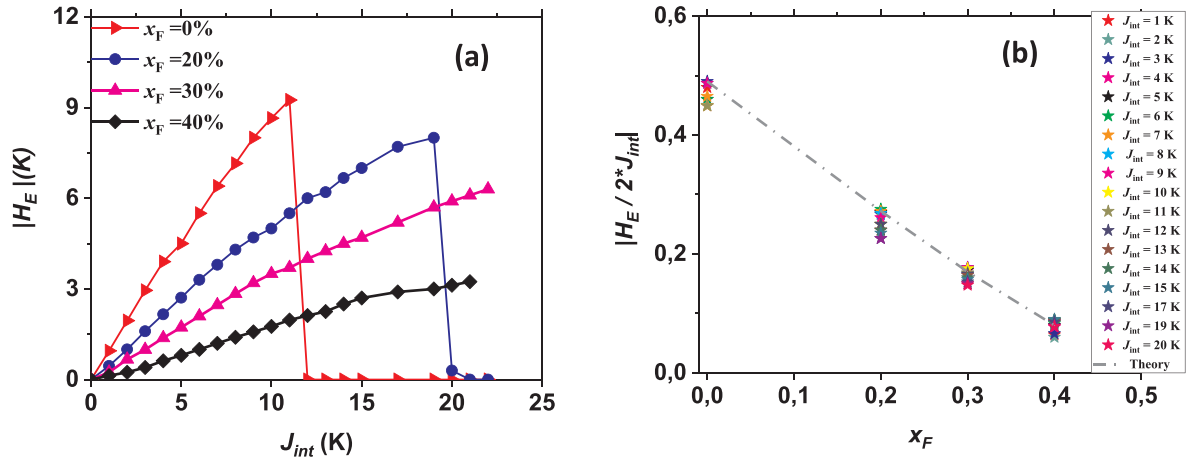


Fig. 15. (a) Variation of H_E simulated at 0.1 K versus J_{int} for $x_F < x_c \approx 50\%$, and (b) variation of $\mu_0 \mu_B g_F |H_E| / (4 S_{AF} J_{int})$ versus $x_F < x_c$ in comparison with the theoretical curve ($J_2^{AF} = 0$ K).

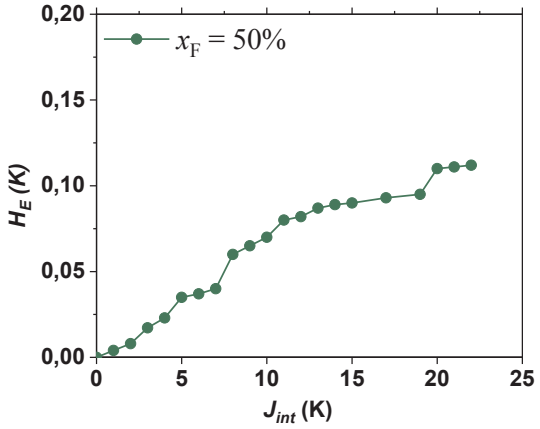


Fig. 16. Variation of H_E simulated at 0.1 K versus J_{int} for $x_F = 50\%$ ($J_2^{AF} = 0$ K).

results provide evidence that roughness at the F/AF interface can reduce drastically the exchange field leading to values which are of the same order of magnitude as experimental values. We also mention as a conclusion that, in our model, the non-collinear magnetic configurations are always confined in the first plane of the AF layer and we did not observe canted magnetic moments in the bulk of the AF layer. The issue of how and why these non-collinear configurations can develop in the AF layer should be addressed in a near future.

Declaration of Competing Interest

The authors declare that they have no known competing financial interests or personal relationships that could have appeared to influence the work reported in this paper.

Acknowledgements

This project is funded by the Région Normandie and the European Union. Europe invests in Normandy with the European Regional Developement Fund (ERDF) – MAGMA project. The authors acknowledge the Centre Régional Informatique et d'Applications Numériques de Normandie (CRIANN) where simulations were performed as Project No. 2010006.

References

[1] W.H. Meiklejohn, C.P. Bean, Phys. Rev. 102 (1956) 1413.
[2] J. Noguès, I.K. Schuller, J. Magn. Magn. Mater. 192 (1999) 203.
[3] A.E. Berkowitz, K. Takano, J. Magn. Magn. Mater. 200 (1999) 552.
[4] V. Baltz, A. Manchon, M. Tsoi, T. Moriyama, T. Ono, Y. Tserkovnyak, Rev. Mod. Phys. 90 (2018) 015005.
[5] I.L. Prejbeanu, M. Kerekes, R.C. Sousa, H. Sibuet, O. Redon, B. Dieny, J.P. Nozières, J. Phys.: Condens. Matter 19 (2007) 165218.
[6] A. Schuhl, D. Lacour, Comptes Rendus Physique 6 (2005) 945.
[7] S. Parkin, X. Jiang, C. Kaiser, A. Panchula, K. Roche, M. Samant, Proc. IEEE 91 (2003) 661.
[8] R.C. Sousa, I.L. Prejbeanu, Comptes Rendus Physique 6 (2005) 1013.
[9] V. Cros, O. Boulle, J. Grollier, A. Hamzić, M. Muñoz, L.G. Pereira, F. Petroff, Comptes Rendus Physique 6 (2005) 956.
[10] C. Chappert, A. Fert, F. N. Van Dau, nature materials 6 (2007).
[11] B. Dieny, V.S. Speriosu, S. Metin, S.S.P. Parkin, B.A. Gurney, P. Baumgart, D.R. Wilhoit, J. Appl. Phys. 69 (1991) 4774.
[12] J.R. Childress, R.E. Fontana, Comptes Rendus Physique 6 (2005) 997.
[13] J.P. Nozières, Reflets Phys. 12 (2010).
[14] H. Ohldag, A. Scholl, F. Nolting, E. Arenholz, S. Maat, A.T. Young, M. Carey, J. Stöhr, Phys. Rev. Lett. 91 (2003) 017203.
[15] J. Ventura, J.P. Araujo, J.B. Sousa, A. Veloso, P.P. Freitas, J. Appl. Phys. 101 (2007) 113901.
[16] V. Baltz, G. Gaudin, P. Somani, B. Dieny, Appl. Phys. Lett. 96 (2010) 262505.
[17] V. Baltz, B. Rodmacq, A. Zarefy, L. Lechevallier, B. Dieny, Phys. Rev. B 81 (2010) 052404.
[18] K. Akmaldinov, S. Auffret, I. Joumard, B. Dieny, V. Baltz, Appl. Phys. Lett. 103 (2013) 042415.
[19] M.P. Proenca, J. Ventura, C.T. Sousa, M. Vazquez, J.P. Araujo, Phys. Rev. B 87 (2013) 134404.
[20] F. Spizzo, E. Bonfiglioli, M. Tamisari, A. Gerardino, G. Barucca, A. Notargiacomo, F. Chinni, L. Del Bianco, Phys. Rev. B 91 (2015) 064410.
[21] V.P. Nascimento, E.C. Passamani, A.D. Alvarenga, F. Pelegrini, A. Biondo, E. Baggio Saitovitch, J. Magn. Magn. Mater. 320 (2008) e272.
[22] R. Wu, M. Xue, T. Maity, Y. Peng, S.K. Giri, G. Tian, J.L. MacManus-Driscoll, J. Yang, Phys. Rev. B 101 (2020) 014425.
[23] G. Lhoutellier, D. Ledue, R. Patte, F. Barbe, B. Dieny, V. Baltz, J. Phys. D: Appl. Phys. 48 (2015) 115001.
[24] G. Lhoutellier, D. Ledue, R. Patte, V. Baltz, J. Appl. Phys. 120 (2016) 193902.
[25] H. Kanso, R. Patte, V. Baltz, D. Ledue, Phys. Rev. B 99 (2019) 054410.
[26] H. Kanso, R. Patte, D. Ledue, J. Magn. Magn. Mater. 491 (2019) 165543.
[27] O.V. Billoni, S.A. Cannas, F.A. Tamarit, J. Phys.: Condens. Matter 23 (2011) 386004.
[28] M.D. Stiles, R.D. McMichael, Phys. Rev. B 59 (1999) 3722.
[29] P. Miltényi, M. Gierlings, J. Keller, B. Beschoten, G. Güntherodt, U. Nowak, K.D. Usadel, Phys. Rev. Lett. 84 (2000) 4224.
[30] U. Nowak, K.D. Usadel, J. Keller, P. Miltényi, B. Beschoten, G. Güntherodt, Phys. Rev. B 66 (2002) 014430.
[31] J. Spray, U. Nowak, J. Phys. D: Appl. Phys. 39 (2006) 4536.
[32] J.D. Agudelo-Giraldo, E. Restrepo-Parra, J. Restrepo, Physica B: Condensed Matter 434 (2014) 149.
[33] J. Moritz, P. Bacher, B. Dieny, Phys. Rev. B 94 (2016) 104425.
[34] Y. Yüksel, Physics Letters A 382 (2018) 1298.
[35] J. Camarero, Y. Pennec, J. Vogel, M. Bonfim, S. Pizzini, F. Ernult, F. Fettar, F. Garcia, F. Lançon, L. Billard, B. Dieny, A. Tagliaferri, N.B. Brookes, Phys. Rev. Lett. 91 (2003) 027201.
[36] A.P. Malozemoff, Phys. Rev. B 35 (1987) 3679.
[37] A.P. Malozemoff, Phys. Rev. B 37 (1988) 7673.

[38] A.P. Malozemoff, J. Appl. Phys. 63 (1988) 3874.
[39] K.D. Usadel, U. Nowak, Phys. Rev. B 80 (2009) 014418.
[40] D.P. Landa, K. Binder, A Guide to Monte Carlo Simulations in Statistical Physics, Cambridge University Press, Cambridge, England, 2008.
[41] M. Lavrskyi, H. Zapolsky, A.G. Khachaturyan, Npj Comput. Mater. (2016).
[42] A.G. Khachaturyan, Theory of Structural Transformations In Solids, Wiley, 1983.
[43] O. Kapikranian, H. Zapolsky, R. Patte, C. Pareige, B. Radiguet, P. Pareige, Phys. Rev. B 92 (2015) 224106.
[44] N. Mavrikakis, C. Detlefs, P.K. Cook, M. Kutsal, A.P.C. Campos, M. Gauvin, P.R. Calvillo, W. Saikaly, R. Hubert, H.F. Poulsen, A. Vaugeois, H. Zapolsky, D. Mangelinck, M. Dumont, C. Yildirim, Acta Mater. 174 (2019) 92.
[45] A.P. Sutton, V. Vitek, Philos. Trans. R. Soc. A 309 (1983) 1506.
[46] J.M.D. Coey, Magnetism and Magnetic Materials, Cambridge University Press, Cambridge, England, 2010.
[47] K. Chen, A.M. Ferrenberg, D.P. Landau, Phys. Rev. B 48 (1993) 3249.
[48] E. du Trémolet de Lacheisserie, Magnétisme, Matériaux et Applications 2000 Collection Grenoble Sciences EDP Sciences, Les Ulis, France.
[49] N. Metropolis, A.W. Rosenbluth, M.N. Rosenbluth, A.H. Teller, E. Teller, J. Chem. Phys. 21 (1953) 1087.
[50] U. Nowak, R.W. Chantrell, E.C. Kennedy, Phys. Rev. Lett. 84 (2000) 163.
[51] O. Chubykalo, U. Nowak, R. Smirnov-Rueda, M.A. Wongsam, R.W. Chantrell, J.M. Gonzalez, Phys. Rev. B 67 (2003) 064422.